

Environmental Dependence of the Structure of Brightest Cluster Galaxies

S. Brough,^{1,2*} C. A. Collins,¹ D. J. Burke,³ P. D. Lynam⁴, R. G. Mann⁵

¹*Astrophysics Research Institute, Liverpool John Moores University, Egerton Wharf, Birkenhead, CH41 1LD, UK*

²*Centre for Astrophysics and Supercomputing, Swinburne University of Technology, Hawthorn, VIC 3122, Australia*

³*Harvard-Smithsonian Center for Astrophysics, 60 Garden Street, Cambridge, MA 02138, USA*

⁴*European Southern Observatory, Casilla 19001, Santiago 19, Chile*

⁵*Institute for Astronomy, University of Edinburgh, Royal Observatory, Blackford Hill, Edinburgh, EH9 3NJ, UK*

Accepted... Received...; in original form 2005

ABSTRACT

We measure the Petrosian structural properties of 33 brightest cluster galaxies (BCGs) at redshifts $z \leq 0.1$ in X-ray selected clusters with a wide range of X-ray luminosities. We find that some BCGs show distinct signatures in their Petrosian profiles, likely to be due to cD haloes. We also find that BCGs in high X-ray luminosity clusters have shallower surface brightness profiles than those in low X-ray luminosity clusters. This suggests that the BCGs in high X-ray luminosity clusters have undergone up to twice as many equal-mass mergers in their past as those in low X-ray luminosity clusters. This is qualitatively consistent with the predictions of hierarchical structure formation.

Key words: Galaxies: clusters: general – galaxies: elliptical and lenticular, cD – galaxies: evolution – galaxies: formation

1 INTRODUCTION

The first-ranked or brightest cluster galaxies (BCGs) are uniquely positioned at the centre of the gravitational potential of clusters of galaxies. With brightnesses roughly ten times that of L^* galaxies, BCGs are not simply the bright extension of a Schechter luminosity function (e.g. Sandage 1976; Tremaine & Richstone 1977; Bernstein & Bhavsar 2001). They are predominantly elliptical in their morphology and owing to their extreme luminosities and position, they dominate their host cluster visually, forming a unique population in their own right. However, their evolution and how their environment affects that evolution, are still poorly understood.

In previous papers of this series on the K-band photometric properties of BCGs; Collins & Mann (1998); Burke et al. (2000) and Brough et al. (2002): we observe that BCGs in clusters with an X-ray luminosity $L_X > 1.9 \times 10^{44}$ erg s⁻¹ (in the EMSS passband 0.3–3.5 keV with $\Omega_\Lambda = 0.7$, $\Omega_m = 0.3$, $h = 0.7$) are brighter and more uniform than those in their low X-ray luminosity counterparts at redshifts $z \geq 0.1$. It appears from Brough et al. (2002) that the evolutionary history of BCGs depends on the richness of their cluster environment, with BCGs in the most luminous clusters showing little sign of merging since $z \sim 1$

and those in the least luminous clusters showing significant signs of mass growth over the same timescale. However, the mass accretion rates inferred in Brough et al. (2002) rely on the assumption that increases in luminosity are attributable to increases in mass.

It is important to confirm this result to determine whether the mass evolution of BCGs is dependent on their environment. If BCGs are in dynamical equilibrium then changes in mass should produce changes in size. Therefore, a means to test the assumption of increases in luminosity being attributable to mass accretion, and confirm the results from Brough et al. (2002), is to measure the structural parameters (size and surface brightness) of BCGs with respect to the properties of their host cluster environment.

Many authors have studied the effects of mergers on galaxy surface brightness profiles since Toomre & Toomre (1972) suggested that dynamical friction, and the consequent merging, of pairs of disc galaxies could form elliptical galaxies. Numerical simulations indicate that the de Vaucouleurs $r^{1/4}$ surface brightness profile (de Vaucouleurs 1948) is robust to the effects of mergers (Barnes 1988; Navarro 1990). The profile of the remnant is only disturbed with respect to the de Vaucouleurs prediction at radii greater than the effective radius and these disturbances move outwards with time, disappearing within the dynamical timescale of the galaxy. Schweizer (1982) observed that the V-band light distribution of NGC7252, a galaxy which appears to

* Email: sbrough@astro.swin.edu.au

have undergone a recent merger, had already established an $r^{\frac{1}{4}}$ profile. Wright et al. (1990); James et al. (1999) and Brown et al. (2003) examined K -band surface brightness profiles of merger galaxies and merger remnants, all confirming that the structure of the mergers more closely resembled that of elliptical galaxies than spiral bulges.

More recently, mergers between elliptical galaxies have been simulated in order to understand the observed tilt of the Fundamental Plane (FP; between radius, surface brightness and velocity dispersion) with respect to the Virial theorem. These simulations find that the effective radius of merger remnants increases with total mass – (e.g. Navarro 1990; Capaccioli et al. 1992; Capelato et al. 1995; Dantas et al. 2003; Evstigneeva et al. 2004), with the surface brightness, consequently, decreasing. Equal-mass dissipationless merging of simulated elliptical galaxies produces structurally non-homologous remnants and is, therefore, able to reproduce the observed FP (Capelato et al. 1995; Nipoti et al. 2003). These studies suggest that galaxies become larger and more diffuse as a function of merger events.

Observations of the Kormendy relation (between radius and surface brightness; Kormendy 1977) of BCGs show that they lie off the relationship followed by normal cluster elliptical galaxies, having larger radii and lower mean surface brightnesses than is predicted by simply scaling the relationships followed by normal elliptical galaxies (Thuan & Romanishin 1981; Hoessel et al. 1987; Schombert 1987; Oegerle & Hoessel 1991). However, they do lie on the same FP as normal cluster ellipticals (Oegerle & Hoessel 1991). These observations are consistent with the suggestion that BCGs have undergone an increased merger history with respect to normal cluster elliptical galaxies. There are also suggestions that the de Vaucouleurs effective radii of BCGs correlate with their environment. Garilli et al. (1997) fitted de Vaucouleurs $r^{\frac{1}{4}}$ laws to the surface brightness profiles of 17 BCGs with redshifts $z < 0.2$ in the g -, r - and i -bands. They find a correlation between effective radius and local galaxy density (measured as the number of galaxies brighter than $M_V = -18$ in circles of projected radii equal to 200 kpc) in the sense that larger BCGs are found in environments which are locally denser at the present epoch. Few other studies have taken environment into account so it is unclear what role environment plays in the structural differences observed between normal cluster elliptical galaxies and BCGs.

In this paper the structural properties of BCGs are measured to further examine how the properties of BCGs depend on their host cluster environment, with the aim of interpreting their evolutionary history. This analysis uses a larger sample of objects covering a significantly wider range in environmental density than previous studies. An objective measure of environmental density is vitally important in any study of BCG properties. As the cluster X-ray luminosity is proportional to the volume integral of the square of the density of the intra-cluster medium it provides a quantitative measure of the environmental density of BCGs with which to analyse possible environmental dependences. We also make use of near-infrared imaging with its associated benefits of small evolutionary corrections and low Galactic extinction

The sample is outlined in Section 2 along with a description of the reduction of the data. The analysis techniques are presented in Section 3. The results obtained are introduced in Section 4 and discussed in Section 5 and the conclusions drawn from this paper are presented in Section 6.

2 DATA

2.1 Sample

Following on from the photometric analysis in Brough et al. (2002) the aim was to construct a sample of BCGs in X-ray selected clusters with a wide range of X-ray luminosities. Structural analysis requires high resolution images and to achieve this our analysis is primarily concerned with the structural properties of BCGs at redshifts $z \leq 0.1$.

The Burke et al. (2000) sample consists of 78 BCGs with redshifts $0.0 < z < 0.8$ in clusters selected from Einstein Medium-Sensitivity Survey (EMSS; Gioia & Luppino 1994) and the Serendipitous High-redshift Archival ROSAT Cluster (SHARC; Burke et al. 1997, 2003; Romer et al. 2000) X-ray cluster catalogues. These galaxies were observed in the K -band with the Infra-Red CAMera 3 (IRCAM3) on the United Kingdom Infra-Red Telescope (henceforth UKIRT; 1 pixel = $0.281''$ giving a field of view of $72''$) between 1994 and 1998. Eleven of these BCGs are at redshifts $z < 0.1$ (all from the EMSS catalogue) and, therefore, suitable for use in this analysis.

In contrast to the analysis in Brough et al. (2002) it was not possible to use the 2MASS extended source catalogue (Jarrett et al. 2000) for this analysis. 2MASS only provides one surface brightness measurement and the two images it provides are not adequate for a structural analysis: The postage stamp images are scaled to the size of the galaxy and are too small to analyse to a reasonable radius. The images from the actual scans, have a scale of $1''/\text{pixel}$ which is too large to provide a meaningful analysis.

Therefore, to extend this analysis a further 26 BCGs with redshifts $0.04 < z < 0.1$ selected from the Lynam catalogue (Lynam 1999) were observed over 3 nights (14-16 January 2001) in the K_n -band with the QUick Infra-Red Camera (QUIRC) on the University of Hawaii 2.2m telescope (henceforth UH; 1 pixel = $0.189''$ giving a field-of-view of $193''$). These BCGs are in clusters selected from the NOrthern ROSAT All-Sky X-ray cluster survey (NORAS; Böhringer et al. 2000). The UKIRT and UH data were reduced in the same manner and a brief overview of this process is given below.

As there are two galaxies in common between the UH and UKIRT samples (those in the clusters MS0301-7 and MS0904-5) this gives a total sample of 35 BCGs, all with redshifts $z \leq 0.1$.

2.2 Data Reduction

The data reduction was performed using the IRAF/DIMSUM (Deep Infrared Mosaicing Software UM) package.

The individual frames were masked for bad pixels, dark subtracted and divided by the exposure time. A flat field

image was created by median combination of the object images, or separate sky exposures if these were available, and applied to the object frames. Masking of cosmic ray events was performed on the flattened images before they were mosaiced together, which completed the processing of those objects with sky exposures. Otherwise the mosaic, which is substantially deeper than the individual exposures, was used to create an object mask, which was then applied to the individual images before they were median-combined to form a flat. The flattened images were then processed as above to create the final image.

Observations of stars from the UKIRT faint standards list (Casali & Hawarden 1992) were used to calibrate the UKIRT photometry onto the UKIRT system assuming an extinction of 0.088 mag airmass⁻¹, the median value for K-band observations at Mauna Kea.

The UH images were calibrated using observations of standard stars selected from the UKIRT extended faint standards list (Hawarden et al. 2001). At least 7 different standards were observed at least 3 times each night. With little variation over the 3 nights, the observations were combined to give an atmospheric extinction coefficient of 0.118 mag airmass⁻¹ and a zero-point of 23.305 with a standard deviation $\sigma = 0.029$ mag.

3 ANALYSIS

One of the major problems in measuring the structural properties of any galaxy type is systematic errors in the measurement of the sky levels (e.g. Graham et al. 1996; Gonzalez et al. 2001) as even the smallest excess flux can swamp the galaxy flux in the outer annuli, and oversubtraction results in a truncation of the profile. This problem is increased when analysing BCGs, due to their larger size and the fact that, locally, BCGs are observed to have significant amounts of flux in their outer wings (Graham et al. 1996).

In this analysis the sky levels were calculated using SExtractor (Bertin & Arnouts 1996). In this program the sky level is estimated by constructing a grid and estimating the background within each square with a sigma-clipped mean. The grid is then median filtered to remove the effects of large bright objects. A grid size of 64 pixels and a median filter size of 3×3 grid squares was used here in order to avoid the background estimation being affected by the presence of other galaxies. This method was compared with measuring the background by obtaining the median of the counts measured in small annuli at different points around the image, the difference was of the order of 10 per cent in $\sigma_{background}$ calculated by SExtractor and no systematic offsets were observed.

Owing to their position at the centres of clusters of galaxies, BCGs are often surrounded by many other galaxies. It is important not to incorporate the light of these galaxies when measuring the surface brightness profile of the BCG. In order to avoid this problem, the flux from the neighbouring galaxies needs to be carefully excluded from the images. When fitting surface brightness profiles in 2D it is possible to deconvolve each galaxy and subtract the flux due to the curves of growth of the companion galaxies, replacing the actual BCG flux in each excluded pixel with that calculated using its symmetric counterpart about the centre of

the BCG (e.g. Lauer 1986; Garilli et al. 1997; Nelson et al. 2002). However, this assumes that the BCG is symmetric and that there is not a further object affecting the counterpart position.

To reduce systematic uncertainties in this analysis these assumptions were not made. Pixels that were identified as belonging to a contaminating source were excluded from the profile calculation. The exclusion radius around each source was initially set to twice the semi-major axis of the contaminating source (as reported by SExtractor). These apertures were then inspected by eye, and the exclusion radii of those sources close to the BCG centre were reduced, since the BCG flux close to the centre is so high that flux from other galaxies is insignificant.

The galaxies were then fitted with elliptical isophotes using the IRAF task ELLIPSE (Jedrzejewski 1987; e.g. Garilli et al. 1997; Gonzalez et al. 2001) which calculates the *median* intensity within each isophote, further reducing the effect flux from companion galaxies can have on the profile of the BCG. The centres of the ellipses were fixed while the position angles and ellipticities were allowed to vary freely.

ELLIPSE was allowed to run until either the angular extent of an elliptical annulus reached the width of the image or greater than 75 per cent of the pixels in a single annulus were masked out. Intensities differing from the median by more than 2 standard deviations were excluded to ensure the quality of the data being fitted. The radii were then circularized ($r = \sqrt{ab}$) and converted from arcseconds to h^{-1} kpc assuming a WMAP cosmology (Spergel et al. 2003): $\Omega_m = 0.3$, $\Omega_\Lambda = 0.7$ and $H_0 = 100h$ km s⁻¹ Mpc⁻¹ with $h = 0.7$.

3.1 Petrosian Structural Parameters

Petrosian structural parameters (Petrosian 1976) have a number of advantages over those calculated from fits of models (e.g. de Vaucouleurs law, Sérsic law) to the surface brightness profile. In particular, no assumption of the stellar light distribution is made in their calculation, making them a direct measure of galaxy properties, from the local surface brightness. The Petrosian parameters are also relatively insensitive to zero-point errors and errors in the extinction correction, as is clear from the Petrosian relationship:

$$\eta(r) = \mu(r) - \langle \mu(r) \rangle, \quad (1)$$

where $\mu(r)$ is the surface brightness (in magnitudes) at a radius r and $\langle \mu(r) \rangle$ is the mean surface brightness within r .

Figure 1 shows some example $\eta(r)$ profiles. The error bars indicate the 1σ statistical errors on η calculated by combining the measured errors on $\mu(r)$ and $\langle \mu(r) \rangle$ in quadrature.

The Petrosian radii and surface brightness can be measured from the η profile at a chosen value of η . The choice of η value to use depends on the sample: r_η should be large enough to be unaffected by seeing ($\eta \geq 1.5$; Sandage & Perelmuter 1990a) but not so large that the surface brightnesses are noisy and unduly sensitive to sky subtraction errors. Figure 1 illustrates that the errors on the η parameter increase with η , and Kjærgaard et al. (1993) find larger errors in their r_η at $\eta = 2$ than at $\eta = 1.5$. The images for this analysis have seeing of $\sim 1.5''$ and the images have

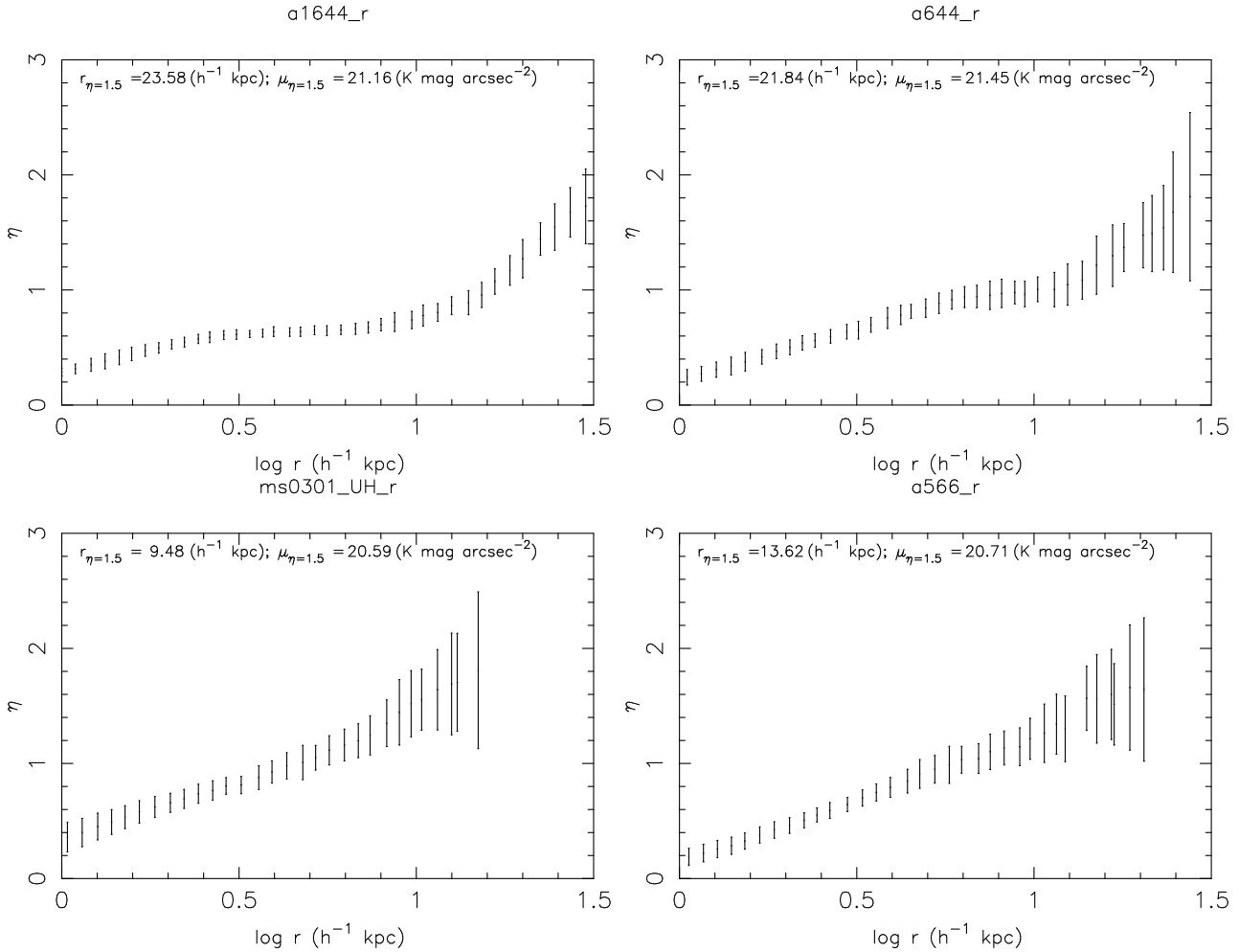


Figure 1. Example $\eta(r)$ profiles of the BCGs in A1644, A644 (both high X-ray luminosity clusters), and those in MS0301-7 and A566 (both low X-ray luminosity clusters). The caption on each panel gives the Petrosian radius, r_η , and surface brightness, μ_η , measured from each profile at $\eta = 1.5$. The error bars indicate the 1σ statistical errors on η calculated by combining the measured errors on $\mu(r)$ and $\langle\mu(r)\rangle$ in quadrature.

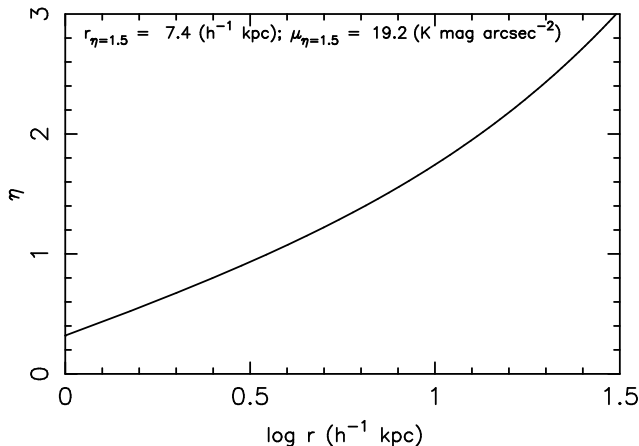


Figure 2. Example $\eta(r)$ profile for a model galaxy following a perfect de Vaucouleurs law ($r_e = 5 h^{-1}$ kpc; $\mu_e = 17.8$ mag arcsec $^{-2}$).

typical limiting depths of $K \sim 22$ mag arcsec $^{-2}$, therefore, Petrosian parameters calculated at $\eta = 1.5$ satisfy both of these requirements. This results in a sample of BCGs with Petrosian radii in the range $7'' < r_{\eta=1.5} < 37''$ and surface brightnesses 19.5 mag arcsec $^{-2} < \mu_{\eta=1.5} < 22.0$ mag arcsec $^{-2}$.

The average Petrosian surface brightness $\langle\mu_\eta\rangle$ was calculated by summing the counts within r_η and averaging over the area enclosed. $\langle\mu_\eta\rangle$ was then corrected for cosmological dimming ($[1+z]^4$) and Galactic absorption using the maps of Schlegel et al. (1998); the absorption correction is small, typically ~ 0.02 mag. The surface brightnesses were also K-corrected using model predictions from the GISEL96 code (Bruzual & Charlot 1993), following Yoshii & Takahara (1988). These K-corrections also include an evolutionary correction, assuming pure luminosity evolution from a redshift of formation, $z_f = 2$. The results are unchanged if the formation redshift is increased to $z_f = 5$.

The effects of masking companion galaxies and excluding points with large errors in their intensities mean that it was not possible to calculate $r_{\eta=1.5}$ for 2 out of the 35

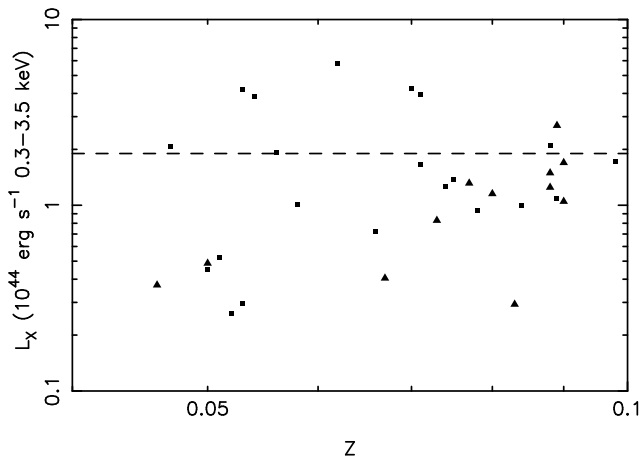


Figure 3. The distribution of cluster X-ray luminosity with redshift for the host clusters of the 33 BCGs studied here. The squares indicate clusters selected from the NORAS X-ray cluster catalogue (Böhringer et al. 2000), the triangles indicate those selected from the EMSS X-ray cluster catalogue (Gioia & Luppino 1994). The dashed line indicates a cluster X-ray luminosity of $L_X = 1.9 \times 10^{44} \text{ erg s}^{-1}$, defined as marking the division between the two populations of BCGs at redshifts $z > 0.1$.

BCGs in this sample, both in clusters with X-ray luminosities $< 1.9 \times 10^{44} \text{ erg s}^{-1}$. This leaves a total sample of 33 BCGs with $0.04 < z < 0.1$ in clusters with X-ray luminosities $0.26 \times 10^{44} < L_X \text{ erg s}^{-1} < 5.8 \times 10^{44}$. The distribution of the X-ray luminosities of the host clusters of these 33 BCGs is shown in Figure 3. This illustrates both the range of host cluster environment covered, over one order of magnitude in X-ray luminosity, and that this range remains consistent over the redshift range studied. The Petrosian structural parameters for these 33 BCGs are given in Table 1.

Statistical errors on the measurement of r_η and $\langle \mu_\eta \rangle$ were calculated by Monte Carlo realisations of the η profile. The profile was resampled from a series of Gaussian profiles each with a FWHM equal to the rms of each point, and the parameters measured for each resampled profile. This process was repeated 1000 times resulting in 1000 independent measurements of each parameter, and, therefore, the spread around them. The standard deviation around the re-sampled parameters is of the order of 10 per cent in r_η and $\Delta \langle \mu_\eta \rangle \sim 0.4 \text{ mag arcsec}^{-2}$.

3.2 Consistency

It is possible to check the consistency of the analysis methods described above as repeat observations were made with both telescopes.

Table 2 summarises the Petrosian parameters measured for the three BCGs with repeat observations made by UH and the two BCGs with repeat observations made by UKIRT. Two galaxies (those in the clusters MS0301-7 and MS0904-5) were observed by both UH and UKIRT, enabling a comparison of the photometry between the two telescopes. The 5 galaxies have a mean absolute difference $\Delta \bar{r}_\eta = 0.86 \pm 0.27 h^{-1} \text{ kpc}$ and $\Delta \langle \mu_\eta \rangle = 0.20 \pm 0.14 \text{ mag arcsec}^{-2}$. The errors quoted are the error on the mean

($= \sigma/\sqrt{N}$). The difference in $\langle \mu_\eta \rangle$ is comparable to the statistical errors, however the statistical error on r_η is significantly larger.

These comparisons confirm that there are no significant offsets between the observations made on different nights or with the different telescopes. This also demonstrates the stability of the parameters fitted and the validity of the analysis techniques used.

4 RESULTS

Two of the BCGs in Figure 1 (those in Abell 644 and Abell 1644) clearly show a plateau in their η profiles. This has been observed previously by Kjærgaard et al. (1993) in NGC 4874, one of the two BCGs in Coma, which is known to have a cD morphology. This plateau is not present in the profiles of normal cluster elliptical galaxies that follow perfect de Vaucouleurs laws (Figure 2; Sandage & Perlmutter 1990a,b, 1991; Kjærgaard et al. 1993). Abell 644 and Abell 1644 have been classified as cD clusters by Struble & Rood (1987), however, the BCGs themselves have not yet been individually classified as cD galaxies. The plateaux we observe are analogous to those observed by Kjærgaard et al. (1993) in NGC 4874. We therefore speculate that the plateaux are likely to be a signature of the cD morphology. The detailed study of the profiles of cD galaxies by Schombert (1988) suggests that the envelopes of cD galaxies become dominant over the underlying galaxy component at an absolute surface brightness $\sim \mu_V \geq 24 \text{ mag arcsec}^{-2}$, this is evident as a break in the surface brightness profile at these surface brightnesses. Assuming a $V - K$ colour $\sim 3.0 \text{ mag}$ from Bower et al. (1992), this corresponds to $\mu_K \geq 21 \text{ mag arcsec}^{-2}$ for these data. The plateaux in these data begin at $r \sim 10 h^{-1} \text{ kpc}$ and $\mu_K \sim 19 \text{ mag arcsec}^{-2}$ suggesting that the halo of BCGs with cD morphologies is distinguishable at higher surface brightnesses than found previously.

The form of the Petrosian profile indicates a possible fundamental difference between galaxies with cD morphologies and those that follow de Vaucouleurs profiles. The signal-to-noise ratio of these data preclude further analysis of BCGs with cD morphologies, and it is not studied further. However, it is noted that the Petrosian profile could provide an objective means with which to determine cD morphology without obtaining very deep imaging or fitting empirical models, which do not provide an adequate fit (Figure 1, Figure 2; Graham et al. 1996). However, this requires further examination.

The Petrosian Kormendy relationship is shown for all 33 galaxies in Figure 4. The error bars show the statistical errors on these measurements. To illustrate any environmental dependence of BCG properties on the Kormendy relation, the cluster X-ray luminosity, $L_X = 1.9 \times 10^{44} \text{ erg s}^{-1}$ in the EMSS (0.3-3.5 keV) passband, defined in Brough et al. (2002) as marking the division between the two populations of BCGs at redshifts $z > 0.1$, is used. There is an offset between the properties of the BCGs on this relation, depending on their host cluster environment, but they both follow the same relationship. The best-fit Kormendy relation is given by:

$$\langle \mu_\eta \rangle = 2.60^{(0.03)} \log_{10} r_\eta - 16.07^{(0.6)}. \quad (2)$$

Table 1. The Petrosian structural properties. $\langle\mu_\eta\rangle$ is corrected for K-dimming, cosmological dimming and Galactic absorption as described in the text.

Cluster	z	L_X $\times 10^{44} \text{erg s}^{-1}$	$r_{\eta=1.5}$ $h^{-1} \text{kpc}$	$\Delta r_{\eta=1.5}$ $h^{-1} \text{kpc}$	$r_{\eta=1.5}$ arcsec	$\langle\mu_{\eta=1.5}\rangle$ mag arcsec $^{-2}$	$\Delta\langle\mu_{\eta=1.5}\rangle$ mag arcsec $^{-2}$
A133	0.056	1.912	15.53	1.85	20.20	18.64	0.21
A292	0.066	0.720	16.26	1.87	18.22	18.58	0.21
A399	0.071	3.960	26.17	3.17	27.43	19.38	0.27
A401	0.074	1.263	27.07	3.15	27.22	19.72	0.21
A478	0.088	2.095	19.57	2.19	16.97	19.57	0.21
A566	0.098	1.714	13.62	1.88	10.71	19.13	0.25
A644	0.070	4.246	21.84	2.70	23.22	19.90	0.24
A671	0.050	0.451	19.65	2.76	28.60	19.30	0.24
A754	0.053	4.190	16.66	1.87	22.88	18.53	0.20
A757	0.051	0.523	5.96	0.59	8.46	18.34	0.17
A763	0.084	0.996	8.84	1.32	7.96	19.15	0.31
A780	0.054	3.870	14.72	1.41	20.02	19.28	0.16
A970	0.058	1.009	5.98	1.01	7.52	17.99	0.34
A978	0.052	0.260	12.62	2.39	17.55	18.72	0.37
A1291	0.053	0.296	16.85	1.59	23.12	20.49	0.26
A1541	0.089	1.088	24.38	3.18	20.91	19.84	0.27
A1644	0.047	2.073	23.58	2.21	36.32	19.63	0.16
A1775	0.071	1.653	29.27	2.84	30.61	20.20	0.26
A1795	0.062	5.797	22.80	3.42	27.17	20.06	0.34
A1800	0.075	1.379	18.94	2.06	18.89	18.76	0.19
A1809	0.078	0.940	12.86	1.71	12.32	18.65	0.24
MS0007-2	0.050	0.487	11.62	1.50	16.98	18.58	0.24
MS0102-3	0.080	1.154	10.35	1.55	9.79	18.11	0.29
MS0301-7	0.083	0.293	10.50	1.78	9.60	18.91	0.29
MS0904-5	0.073	0.829	11.76	1.63	12.09	18.32	0.26
MS1306-7	0.088	1.494	15.63	4.01	13.68	18.64	0.30
MS1531-2	0.067	0.405	8.06	1.00	8.98	18.44	0.21
MS1558-5	0.088	1.249	19.19	1.62	16.66	19.38	0.16
MS1754-9	0.077	1.315	10.36	1.75	10.14	17.97	0.36
MS2215-7	0.090	1.049	14.42	2.27	12.27	19.32	0.32
MS2216-0	0.090	1.697	21.65	2.34	18.42	19.39	0.22
MS2318-7	0.089	2.688	19.40	1.66	16.67	18.95	0.16
MS2354-4	0.046	0.372	13.06	0.85	20.65	18.41	0.11

Table 3. Kormendy relations fitted to BCG Petrosian structural parameters, the relationships are of the form $\langle\mu_\eta\rangle = M \times \log_{10} r_\eta + C$.

Author	N	λ	M	C	σ
Sandage & Perelmuter (1991)	56	V	3.12	8.51	0.27
Kjærgaard et al. (1993)	18	V	2.11	18.23	0.31
Kjærgaard et al. (1993)	18	B	2.09	19.45	0.29
This sample	33	K	2.60	15.9	0.42

The quantities in brackets are the standard deviations around the gradient and intercept solutions. The scatter around the relation, $\sigma = 0.42 \text{ mag arcsec}^{-2}$.

The Kormendy relations fitted to other samples of Petrosian structural parameters are summarised in Table 3. This sample follows a similar gradient to those fitted by Sandage & Perelmuter (1991) and Kjærgaard et al. (1993) to samples of BCGs, although it has a slightly larger scatter with $\sigma = 0.42 \text{ mag arcsec}^{-2}$ in contrast to $\sigma \sim 0.3 \text{ mag arcsec}^{-2}$.

Table 4. Statistical properties of the BCG Petrosian effective radii, r_η ($h^{-1} \text{kpc}$), and mean surface brightness, $\langle\mu_\eta\rangle$ ($K \text{ mag arcsec}^{-2}$), as a function of cluster X-ray luminosity, L_X .

$L_X (\times 10^{44} \text{erg s}^{-1})$	N	$r_\eta (1\sigma)$	$\langle\mu_\eta\rangle (1\sigma)$
< 1.9	24	14.96 (6.23)	18.93 (0.68)
> 1.9	9	20.03 (3.90)	19.33 (0.53)

To examine the environmental dependence of these parameters further the means and dispersions (split by the X-ray luminosity of their host cluster) are summarised in Table 4.

Figure 5 illustrates the distributions of the BCG Petrosian radii (upper panel) and surface brightnesses (lower panel) as a function of their host cluster environment. A Spearman rank correlation on the Petrosian radii confirms that the BCG radii are correlated with their host cluster environment, with a correlation coefficient of $r_s = 0.55$. For 33 galaxies, the Student's t-test rejects the null hypothesis that there is no correlation at > 99 per cent confidence level. A weighted straight-line fit takes the statistical errors in r_η

Table 2. Summary of the Petrosian parameters measured from repeat observations. The upper table shows the Petrosian radii, r_η (h^{-1} kpc), calculated for each night, the lower table shows the mean Petrosian surface brightness, $\langle\mu_\eta\rangle$ (mag arcsec $^{-2}$).

Cluster	r_η (h^{-1} kpc)						Mean
	8 Nov 1994	9 Nov 1994	11 Jan 1997	14 Jan 2001	15 Jan 2001	16 Jan 2001	
A399				25.99	26.34		26.17
A978				12.48		12.76	12.62
MS0301-7	11.51					9.48	10.50
MS0904-5		11.57	12.47		11.09	11.89	11.76
MS1306-7		15.74	15.52				15.63
Mean Absolute Difference:							0.86±0.27

Cluster	$\langle\mu_\eta\rangle$ (mag arcsec $^{-2}$)						Mean
	8 Nov 1994	9 Nov 1994	11 Jan 1997	14 Jan 2001	15 Jan 2001	16 Jan 2001	
A399				19.43	19.43		19.43
A978				19.02		18.48	18.75
MS0301-7	18.86					19.09	18.98
MS0904-5		18.35	18.46		18.29	18.38	18.40
MS1306-7		18.72	18.69				18.70
Mean Absolute Difference:							0.20±0.14

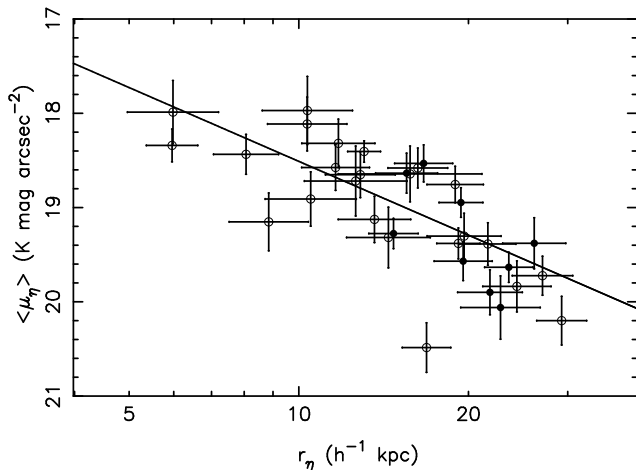


Figure 4. The Petrosian Kormendy relation. The error bars indicate the 1σ statistical errors on the measured parameters. The open points denote BCGs in clusters with $L_X(0.3 - 3.5$ keV) $< 1.9 \times 10^{44}$ erg s $^{-1}$ whilst the filled points denote BCGs in clusters with $L_X(0.3 - 3.5$ keV) $> 1.9 \times 10^{44}$ erg s $^{-1}$. The solid line marks the best-fit relation described by Equation 2.

into consideration and also results in a statistically significant correlation between r_η and L_X :

$$r_\eta = 8.78^{(0.16)} \log_{10} L_X + 12.9^{(2.9)}. \quad (3)$$

This is not a selection effect, Figure 3 illustrates that the host clusters of the BCGs have a uniform distribution in X-ray luminosity over the redshift range of the sample and Section 3.2 demonstrates that there are no offsets between the parameters measured at the different telescopes. The BCG radii are clearly correlated with their host cluster environment.

In contrast, the lower panel of Figure 5 indicates that the Petrosian mean surface brightnesses are not strongly

correlated with their environment. A Spearman rank correlation suggests that the Petrosian surface brightnesses are correlated with their environment with a correlation coefficient $r_s = 0.36$. The Student's t-test rejects the null hypothesis of no correlation at > 95 and < 98 per cent confidence level, suggesting that there is a correlation of $\langle\mu_\eta\rangle$ with environment. A weighted straight-line fit demonstrates that the mean surface brightnesses of BCGs are weakly correlated with their host cluster environment.

$$\langle\mu_\eta\rangle = 0.64^{(0.02)} \log_{10} L_X + 19.0^{(0.3)}. \quad (4)$$

The observed relationships between BCG parameters and those of their host cluster could be due to a systematic error in the background subtraction of these galaxies. In order to test this, the $1\sigma_{background}$ calculated by SEXtractor was used to model the possible systematic errors. This value is typically ~ 2 counts/pixel and is significantly more than the differences between the two background subtraction methods compared in Section 3. The images were reanalysed – first with an extra $1\sigma_{background}$ subtracted and again with $1\sigma_{background}$ added.

The Petrosian profiles of galaxies in those images with $1\sigma_{background}$ added fall off to zero before reaching $\eta = 1.5$ and it is not possible to measure their structural parameters. This is not seen in the original data and is illustrative that the systematic errors are not this large.

The Petrosian radii of BCGs in images with $1\sigma_{background}$ subtracted are smaller and the mean surface brightnesses are brighter than the original measurements. This is illustrated in Figure 6, which also demonstrates that, despite the significant background oversubtraction, the relationships with the Petrosian structural parameters and the X-ray luminosities of their host cluster environments remain. The weighted straight-line fit to the upper panel of Figure 6:

$$r_\eta = 3.93^{(0.06)} \log_{10} L_X + 8.1^{(0.6)}. \quad (5)$$

The weighted straight-line fit to the lower panel of Figure 6:

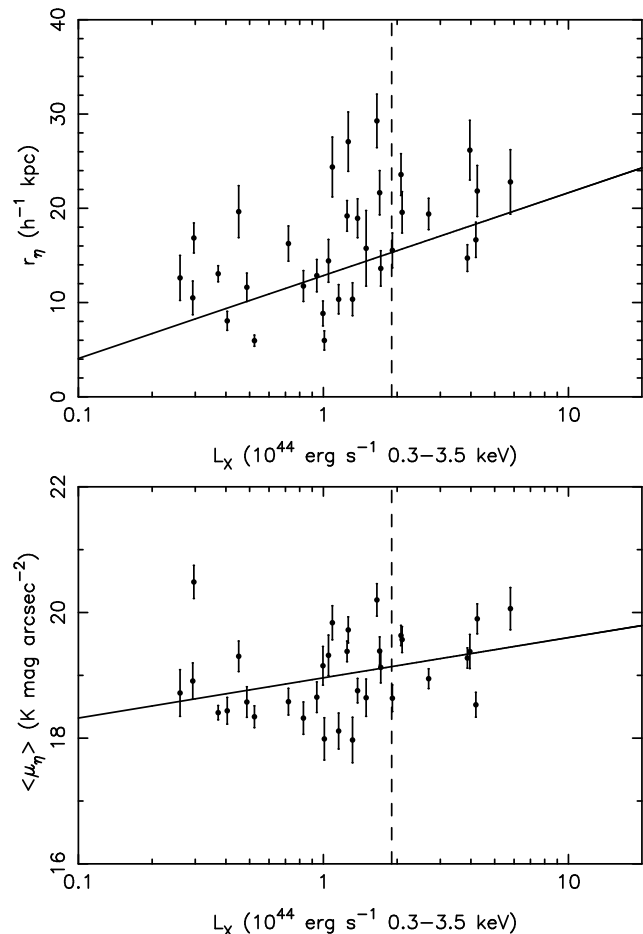


Figure 5. The distribution of Petrosian radius, r_η (upper panel), and mean surface brightness $\langle\mu_\eta\rangle$ (lower panel), with cluster X-ray luminosity, L_X , for 33 BCGs. The error bars indicate the 1σ statistical errors on the parameters. The dashed line indicates the empirical $L_X = 1.9 \times 10^{44} \text{ erg s}^{-1}$ division between high and low X-ray luminosity clusters. The solid line in the upper panel indicates the straight-line fit given by Equation 3, Equation 4 is illustrated by the solid line in the lower panel.

$$\langle\mu_\eta\rangle = 0.44^{(0.01)} \log_{10} L_X + 17.6^{(0.2)}. \quad (6)$$

The BCG parameters are clearly correlated with those of their host cluster environment.

The possibility that the observed relationships between the BCG parameters and those of their environment are due to a systematic error in the background subtraction of these galaxies was further tested by a comparison with Garilli et al. (1997). These authors examined BCGs in the r -band which is less susceptible to problems with background subtraction than the near-infrared, we have 7 BCGs in common.

Garilli et al. (1997) fit de Vaucouleurs profiles to their BCGs and quote the fitted effective radius, r_e , and effective surface brightness, μ_e . Using these values, it is possible to construct the equivalent Petrosian profile for that de Vaucouleurs profile (as seen in Figure 2). First, the effective radius, r_e was transformed into the cosmology used here. The Petrosian radius was then measured at $\eta = 1.5$ as described above. Garilli et al. (1997) do not circularize their profiles

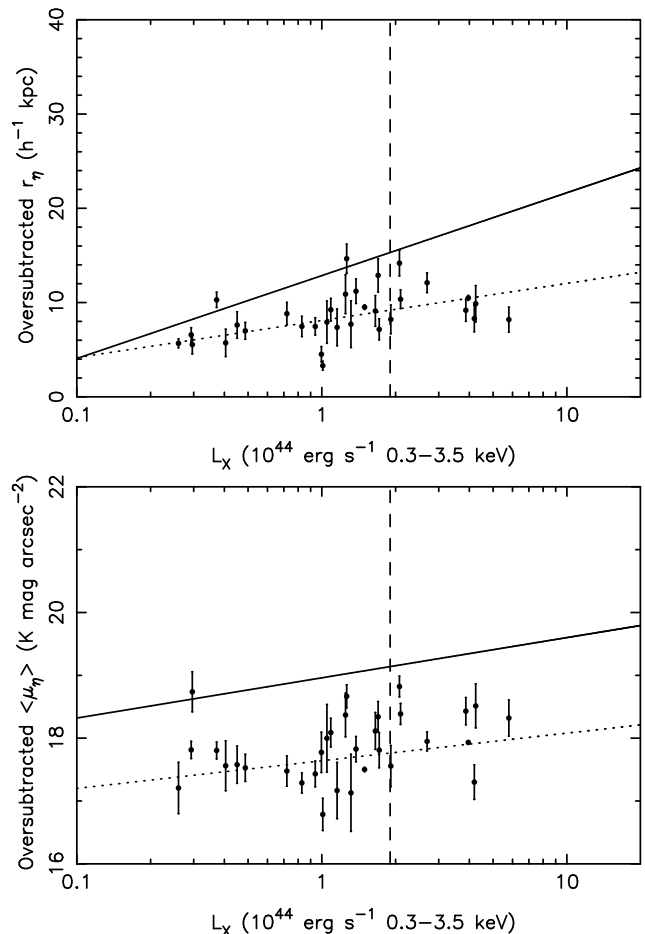


Figure 6. The distribution of Petrosian parameters r_η (upper panel), and mean surface brightness $\langle\mu_\eta\rangle$ (lower panel) measured from images with the background oversubtracted by $1\sigma_{background}$. The error bars indicate the 1σ statistical errors on the parameters. The dashed line indicates the empirical $L_X = 1.9 \times 10^{44} \text{ erg s}^{-1}$ division between high and low X-ray luminosity clusters. The solid line in each panel gives the straight-line fit fitted to the original data, and the dotted line indicates the straight-line fit to the oversubtracted data, described by Equation 5 (upper panel) and Equation 6 (lower panel).

as we have done here so these comparisons are made with the major-axis profiles of these galaxies. It was not, therefore, possible to compare r_η (this work) with r_η (comparison) for the BCG in MS1558-5 as the major-axis profile for this galaxy does not reach $\eta = 1.5$. This leaves a sample of 6 galaxies in common. The measured values are given in Table 5. We also note that the r_η of the BCG in Abell 1644 measured by S. Andreon is in apparent agreement with this work (S. Andreon, private communication).

The mean difference r_η (this work) $- r_\eta$ (comparison) = $-9.3 \pm 5.2 h^{-1} \text{ kpc}$. The most discrepant galaxy is the BCG in Abell 401, with r_η (this work) $- r_\eta$ (comparison) = $33.92 h^{-1} \text{ kpc}$. However, Garilli et al. (1997) note that they determine a de Vaucouleurs effective radius for this BCG which is ~ 25 per cent larger than that obtained by Malumuth & Kirshner (1985) ($r_e = 91.04 \text{ kpc}$). If we discount this galaxy the mean difference between the two samples is then $-4.3 \pm 1.9 h^{-1} \text{ kpc}$. This difference is of the order

Table 5. Comparing major-axis r_η measured from de Vaucouleurs profiles fitted by Garilli et al. (1997) with galaxies in common with this work.

Cluster	r_e h^{-1} kpc	r_η (comp) h^{-1} kpc	r_η (this work) h^{-1} kpc	Δr_η h^{-1} kpc
A399	35.12	44.67	36.20	11.79
A401	59.67	74.67	40.75	6.47
A671	21.74	28.28	23.92	5.67
MS0102-3	9.41	13.01	13.97	3.26
MS0301-7	10.99	15.05	13.92	3.26
MS0904-5	15.66	20.80	12.24	2.61

of the errors on r_η (this work) which are $\Delta r_\eta \sim 4 h^{-1}$ kpc (Table 5). We therefore conclude that the observed relationships are not due to a systematic error in the background calculation of these galaxies.

5 DISCUSSION

In order to understand what the observed correlation between Petrosian radius and host cluster environment means in terms of BCG formation and evolution, the effect that mergers have on the surface brightness profiles of galaxies is considered.

As introduced in Section 1, equal-mass, dissipationless mergers of simulated elliptical galaxies produce structurally non-homologous remnants and are, therefore, able to reproduce the observed FP of elliptical galaxies (Capelato et al. 1995; Nipoti et al. 2003). However, these simulations are unable to reproduce the projections of the FP, the Faber-Jackson and Kormendy relations. The Faber-Jackson relation is characterized by a lower velocity dispersion than predicted by the Faber-Jackson relation for a given luminosity increase and the Kormendy relation by significantly larger radii than predicted from observations (Navarro 1990; Ciotti & van Albada 2001; Nipoti et al. 2003). These simulations are, however, consistent with observations of BCGs. BCGs also lie on the FP for normal cluster elliptical galaxies (Oegerle & Hoessel 1991) but are observed to have significantly lower velocity dispersions than predicted by the Faber-Jackson relation for normal cluster elliptical galaxies (Malumuth & Kirshner 1981, 1985; Oegerle & Hoessel 1991) and larger radii than predicted by the normal cluster elliptical galaxy Kormendy relation (Thuan & Romanishin 1981; Hoessel et al. 1987; Schombert 1987; Oegerle & Hoessel 1991). This suggests that BCGs can form from equal-mass, dissipationless mergers of large luminous elliptical galaxies. However, gas dissipation must be important in the formation of less massive elliptical galaxies in order to increase their central velocities, consistent with the observed Faber-Jackson and Kormendy relations.

Numerical simulations of elliptical galaxy mergers indicate that the effective radii of merger remnants increase proportionally with total mass, by a factor of 1 – 2 (Hoessel 1980; Navarro 1990; Capaccioli et al. 1992; Capelato et al. 1995; Nipoti et al. 2003). There is a range of increase factors because the properties of the remnant are dependent on the energy and angular momentum of the collision as well as the

mass ratios of the progenitors. Head-on, equal-mass dissipationless mergers produce the largest remnants, with effective radii double those of their progenitors (e.g. Capelato et al. 1995; Nipoti et al. 2003). From the predictions of current simulations, the observation that BCGs in high X-ray luminosity clusters are larger, by a factor of ~ 2 , than those in low X-ray luminosity clusters at redshifts $z \leq 0.1$ then suggests that these galaxies have undergone one or two major (equivalent mass) merger events, or several accretion events, more than those BCGs in low- L_X clusters. Figure 1 indicates that BCGs with cD morphologies have larger Petrosian radii than would be measured if they followed perfect de Vaucouleurs profiles. Therefore, the BCG radius – cluster X-ray luminosity relationship could also suggest that there are a higher proportion of BCGs with cD morphologies in high X-ray luminosity clusters than there are in low X-ray luminosity clusters. Higher resolution images would be required to determine this in a non-subjective manner.

Numerical simulations indicate that the density profiles of the remnant galaxies remain the same as those of their progenitors, therefore, the effective surface density should scale as $I_e \propto M_r/r_r^2$ (Navarro 1990). In magnitudes, this corresponds to a change in $\langle \mu_e \rangle$ of up to 1 mag arcsec $^{-2}$ in 2 consecutive equal-mass mergers between elliptical galaxies, as predicted by the simulations of Capelato et al. (1995) and Evstigneeva et al. (2004). The corresponding change in surface brightness predicted is within the observational scatter of this data, explaining the lack of a clear correlation of BCG mean surface brightness with host cluster environment.

Brough et al. (2002) concluded that BCGs in high X-ray luminosity clusters showed little sign of an increase in mass since $z \sim 1$, in contrast to those in low X-ray luminosity clusters which have increased in mass by up to a factor of four over the same timescale. Combining the results presented here with those of Brough et al. (2002) a consistent picture emerges. These two observations suggest that BCGs in high X-ray luminosity clusters assembled their stellar mass at redshifts > 1 and have been passively evolving since, in contrast to those BCGs in low X-ray luminosity clusters which are still in the process of assembling today. This is qualitatively consistent with the theories of hierarchical structure formation which suggest that the less massive systems (clusters and galaxies) we observe today assembled more recently than the most massive systems (e.g. Kauffmann & Charlot 1998).

6 CONCLUSIONS

In this paper, the Petrosian parameters measured from the surface brightness profiles of 33 BCGs in clusters covering a wide range in environmental density have been presented, with the aim of interpreting their evolutionary history.

Analysis of the Petrosian η profiles of this sample indicates that there is a deviation of the Petrosian profiles of some BCGs with cD morphologies from those of a galaxy following a perfect de Vaucouleurs law. This is suggested to be a signature of galaxies with cD morphologies and may indicate a fundamental structural difference.

The structural properties of BCGs are clearly determined by their host cluster environment, as suggested by Garilli et al. (1997). BCGs in high X-ray luminosity clus-

ters are larger and fainter than those in low X-ray luminosity clusters.

Research into other cluster galaxy populations suggests that their properties are driven, not by the global cluster environment, but by their local environment as measured by the density of their nearest neighbours, with those galaxies in the least dense environments, showing the most signs of evolution. The unique position of BCGs means that their local environment *is* the global cluster environment and this affects their evolution such that those BCGs in the least dense environments have undergone more evolution since $z \sim 1$ than those in the most dense clusters. This provides an indication of how a single population of galaxies evolves hierarchically. It is likely that BCGs arise from the merging of satellites, initially drawn towards the cluster centre by collimated infall along filaments in the early epochs of cluster formation, however, this work suggests that this process is continuing in the least dense clusters at the present time.

ACKNOWLEDGMENTS

We thank the referee Stefano Andreon for his valuable suggestions. SB acknowledges PPARC for a Postgraduate Studentship and Phil James, Alfonso Aragón-Salamanca and Dave Carter for helpful comments. DJB acknowledges the support of NASA contract NAS8-39073. We also acknowledge the use of the UH 2.2m telescope at the Mauna Kea Observatory, Institute for Astronomy, University of Hawaii.

REFERENCES

- Barnes, J. E. 1988, *ApJ*, 331, 699
- Bernstein, J. P. & Bhavsar, S. P. 2001, *MNRAS*, 322, 625
- Bertin, E. & Arnouts, S. 1996, *A&AS*, 117, 393
- Böhringer, H., Voges, W., Huchra, J. P., McLean, B., Giacconi, R., Rosati, P., Burg, R., Mader, J., Schuecker, P., Simić, D., Komossa, S., Reiprich, T. H., Retzlaff, J., & Trümper, J. 2000, *ApJS*, 129, 435
- Bower, R. G., Lucey, J. R., & Ellis, R. S. 1992, *MNRAS*, 254, 601
- Brough, S., Collins, C. A., Burke, D. J., Lynam, P. D., & Mann, R. G. 2002, *MNRAS*, 329, 53
- Brown, R. J. N., Forbes, D. A., Silva, D., Helsdon, S. F., Ponman, T. J., Hau, G. K. T., Brodie, J. P., Goudfrooij, P., & Bothun, G. 2003, *MNRAS*, 341, 747
- Bruzual, A. G. & Charlot, S. 1993, *ApJ*, 405, 538
- Burke, D. J., Collins, C. A., & Mann, R. G. 2000, *ApJL*, 532, L105
- Burke, D. J., Collins, C. A., Sharples, R. M., Romer, A. K., Holden, B. P., & Nichol, R. C. 1997, *ApJL*, 488, L8
- Burke, D. J., Collins, C. A., Sharples, R. M., Romer, A. K., & Nichol, R. C. 2003, *MNRAS*, 341, 1093
- Capaccioli, M., Caon, N., & D'Onofrio, M. 1992, *MNRAS*, 259, 323
- Capelato, H. V., de Carvalho, R. R., & Carlberg, R. G. 1995, *ApJ*, 451, 525
- Casali, M. M. & Hawarden, T. G. 1992, *The JCMT-UKIRT Newsletter*, 3, 33
- Ciotti, L. & van Albada, T. S. 2001, *ApJL*, 552, L13
- Collins, C. A. & Mann, R. G. 1998, *MNRAS*, 297, 128
- Dantas, C. C., Capelato, H. V., Ribeiro, A. L. B., & de Carvalho, R. R. 2003, *MNRAS*, 340, 398
- de Vaucouleurs, G. 1948, *Annales d'Astrophysique*, 11, 247
- Evstigneeva, E. A., de Carvalho, R. R., Ribeiro, A. L., & Capelato, H. V. 2004, *MNRAS*, 349, 1052
- Garilli, B., Sangalli, G., Andreon, S., Maccagni, D., Carrasco, L., & Recillas, E. 1997, *AJ*, 113, 1973
- Gioia, I. M. & Luppino, G. A. 1994, *ApJS*, 94, 583
- Gonzalez, A. H., Zaritsky, D., Dalcanton, J. J., & Nelson, A. 2001, *ApJS*, 137, 117
- Graham, A., Lauer, T. R., Colless, M., & Postman, M. 1996, *ApJ*, 465, 534
- Hawarden, T. G., Leggett, S. K., Letawsky, M. B., Ballantyne, D. R., & Casali, M. M. 2001, *MNRAS*, 325, 563
- Hoessel, J. G. 1980, *ApJ*, 241, 493
- Hoessel, J. G., Oegerle, W. R., & Schneider, D. P. 1987, *AJ*, 94, 1111
- James, P., Bate, C., Wells, M., Wright, G., & Doyon, R. 1999, *MNRAS*, 309, 585
- Jarrett, T. H., Chester, T., Cutri, R., Schneider, S., Skrutskie, M., & Huchra, J. P. 2000, *AJ*, 119, 2498
- Jedrzejewski, R. I. 1987, *MNRAS*, 226, 747
- . 1996, *MNRAS*, 280, 167
- Kauffmann, G. & Charlot, S. 1998, *MNRAS*, 297, L23
- Khosroshahi, H. G., Raychaudhury, S., Ponman, T. J., Miles, T. A., & Forbes, D. A. 2004, *MNRAS*, 349, 527
- Kjærgaard, P., Jørgensen, I., & Moles, M. 1993, *ApJ*, 418, 617
- Kormendy, J. 1977, *ApJ*, 218, 333
- Lauer, T. R. 1986, *ApJ*, 311, 34
- Lynam, P. D. L. 1999, Ph.D Thesis, Liverpool John Moores University
- Malumuth, E. M. & Kirshner, R. P. 1981, *ApJ*, 251, 508
- . 1985, *ApJ*, 291, 8
- Navarro, J. F. 1990, *MNRAS*, 242, 311
- Nelson, A. E., Simard, L., Zaritsky, D., Dalcanton, J. J., & Gonzalez, A. H. 2002, *ApJ*, 567, 144
- Nipoti, C., Londrillo, P., & Ciotti, L. 2003, *MNRAS*, 342, 501
- Oegerle, W. R. & Hoessel, J. G. 1991, *ApJ*, 375, 15
- Pahre, M. A. 1998, *AJ*, 116, 1591
- Petrosian, V. 1976, *ApJL*, 209, L1
- Romer, A. K., Nichol, R. C., Holden, B. P., Ulmer, M. P., Pildis, R. A., Merrelli, A. J., Adami, C., Burke, D. J., Collins, C. A., Metevier, A. J., Kron, R. G., & Commons, K. 2000, *ApJS*, 126, 209
- Sandage, A. 1976, *ApJ*, 205, 6
- Sandage, A. & Perlmutter, J. 1990a, *ApJ*, 350, 481
- . 1990b, *ApJ*, 361, 1
- . 1991, *ApJ*, 370, 455
- Schlegel, D. J., Finkbeiner, D. P., & Davis, M. 1998, *ApJ*, 500, 525
- Schombert, J. M. 1987, *ApJS*, 64, 643
- . 1988, *ApJS*, 328, 475
- Schweizer, F. 1982, *ApJ*, 252, 455
- Spergel, D. N., Verde, L., Peiris, H. V., Komatsu, E., Nolta, M. R., Bennett, C. L., Halpern, M., Hinshaw, G., Jarosik, N., Kogut, A., Limon, M., Meyer, S. S., Page, L., Tucker, G. S., Weiland, J. L., Wollack, E., & Wright, E. L. 2003, *ApJS*, 148, 175
- Struble, M. F. & Rood, H. J. 1987, *ApJ*, 323, 468
- Thuan, T. X. & Romanishin, W. 1981, *ApJ*, 248, 439

- Toomre, A. & Toomre, J. 1972, ApJ, 178, 623
Tremaine, S. D. & Richstone, D. O. 1977, ApJ, 212, 311
van Dokkum, P. G. & Stanford, S. A. 2003, ApJ, 585, 78
Wright, G. S., James, P. A., Joseph, R. D., & McLean, I. S.
1990, Nature, 344, 417
Yoshii, Y. & Takahara, F. 1988, ApJ, 326, 1

This paper has been typeset from a \TeX / \LaTeX file prepared by the author.